Journal of Solid State Chemistry **162,** 42–51 (2001)
doi:10.1006/jssc.2001.9339, available online at http://www.idealibrary.com on IDEAL®

Optical and Crystal-Field Analysis of Nd^{3+} Ion in Nd_2BaCuO_5 and Nd_2BaZnO_5

S. A. Klimin,* M. N. Popova,* E. Antic-Fidancev,† and P. Porcher†

Institute of Spectroscopy, Russian Academy of Sciences, 142092 Troitsk, Moscow Region, Russia; and †Laboratoire de Chimie Appliquée de l'Etat Solide, CNRS-UMR7574, ENSCP, 11, Rue Pierre et Marie Curie, 75231 Paris Cedex 05, France

Received March 5, 2001; in revised form July 10, 2001; accepted August 2, 2001

The absorption spectra of neodymium ion in the stoichiometric Nd_2BaCuO_5 and Nd_2BaZnO_5 compounds have been analyzed. The similarity of the spectra is emphasized in spite of apparent differences in the crystal structures and is explained by the same nearest surroundings of the Nd^{3+} ions in both compounds. This circumstance allows us to perform the crystal field calculation on 93 Stark levels coming from the two title compounds. In the fitting procedure a set of 20 free-ion and 9 crystal field phenomenological parameters is obtained with a mean deviation of 13.7 cm^{-1}. Magnetic *g*-factors are computed from the derived wave functions. Exchange splittings of Nd^{3+} levels in a magnetically ordered state of Nd_2BaCuO_5 ($T_N = 7.5$ K) were measured. The experimentally obtained temperature dependence of the exchange splittings reveal quasi-one-dimensional magnetic correlations that persist up to $\sim 10\ T_N$. © 2001 Academic Press

Key Words: **neodymium barium copper–zinc compounds; absorption spectra; crystal field calculations.**

1. INTRODUCTION

The cuprate R_2BaCuO_5 (R is a rare earth or yttrium) is one of the two stable compounds inside the R_2O_3–BaO–CuO phase triangle, the 1-2-3 type high T_c superconductor $RBa_2Cu_3O_{7-x}$ being the other one. The structure of R_2BaCuO_5 with the largest lanthanide ions, namely, with La and Nd, is tetragonal ($P4/mbm$ space group) and the lanthanide ion occupies one C_{2v} symmetry position in the unit cell (1–4). These cuprates are brown in color. The rest of the lanthanide series results in the orthorhombic *Pnma* crystallographic modification with two nonequivalent C_s symmetry positions for R^{3+} ions. These compounds have bright-green color (5). A vast interest for the R_2BaCuO_5 cuprates was first connected with their presence as impurity phases in the 1-2-3 superconducting ceramics. It turned out later that the members of the R_2BaCuO_5 family have interesting magnetic properties (see, e.g., (6–8, 4)). Despite all the efforts, the magnetism of these compounds still is not well understood.

To achieve a better understanding, it is, in particular, important to know the energies and wave functions of crystal field levels for the R^{3+} rare earth ion. The information on crystal field levels of R^{3+} in R_2BaCuO_5 is incomplete, essentially because of the strong absorption bands of d–d transitions in Cu^{2+} ions, which prevent detection of weak f–f lines of R^{3+} ions in optical measurements. The substitution of the magnetic Cu^{2+} ion by a nonmagnetic Zn^{2+} ion seems to be a good solution to the problem. Indeed, our previous comparative study of Er_2BaCuO_5 and Er_2BaZnO_5 (9) has shown that the position of Er^{3+} spectral lines in both compounds are very close in the infrared spectral region where Er_2BaCuO_5 is transparent and, consequently, the positions of crystal field levels can be described by similar sets of crystal field parameters. Both Er_2BaCuO_5 and Er_2BaZnO_5 crystallize in the same structure described by the orthorhombic space group *Pnma* (5, 10). The same is true for R_2BaMO_5 compounds with M = Cu or Zn and R = Sm–Lu and Y (5, 10, 11). In the case of R = Nd, copper and zinc compounds belong to two different space groups, namely, $P4/mbm$ for Nd_2BaCuO_5 (1–4) and $I4/mcm$ for Nd_2BaZnO_5 (12, 13). However, the analysis of the crystal structures (see the next section) shows that the nearest surrounding of the Nd^{3+} ion is similar for both compounds. That permits expectation of the similarity of crystal field and, hence, energy spectra of Nd^{3+} so that spectroscopic data on a transparent nonmagnetic Nd_2BaZnO_5 could be used for a better description of the magnetic Nd_2BaCuO_5.

Earlier optical studies of Nd_2BaZnO_5 were either incomplete or controversial. Taibi *et al.* presented the energy level scheme for Nd^{3+} in Nd_2BaZnO_5 on the basis of absorption measurements in the spectral region between 3800 and 33,800 cm^{-1} and crystal field calculations (14, 15). Later, de Andres *et al.* communicated on the infrared transitions of Nd_2BaZnO_5 between 1800 and 6500 cm^{-1}, from absorption and Raman studies (16) and, then, reinvestigated the spectral region between 1800 and 28,000 cm^{-1} by absorption and emission experiments (17). There are several

0022-4596/01 $35.00

marked discrepancies between the data of Refs. (17) and (15). Rather poor spectroscopic information was available on Nd_2BaCuO_5. Popova and co-workers in their paper communicating the detection of a magnetic phase transition in Nd_2BaCuO_5 at $T_c = 7.5$ K obtained from the analysis of the splittings of Nd^{3+} Kramers doublets (18) reported the crystal field levels of $^4I_{15/2}$ and $^4F_{3/2}$ multiplets. The structure of the $^4I_{15/2}$ and $^4F_{3/2}$ multiplets was reported later in Ref. (17), too.

In this work, we present the absorption spectra of Nd_2BaCuO_5 in the whole transparency window of this compound (1800–18,000 cm^{-1}). Where possible, the exchange splittings of the Nd^{3+} Kramers doublets in a magnetically ordered state of Nd_2BaCuO_5 were determined. The zinc compound was also reinvestigated in the broadest possible spectral region (up to 33,800 cm^{-1}). On the basis of this more complete and reliable data set, we have performed one fitting procedure for both compounds in the framework of the crystal field theory. Thus, obtained wave functions were used to calculate magnetic g-factors of Nd^{3+} levels.

2. CRYSTALLOGRAPHIC BACKGROUND

The crystal structure of both Nd_2BaCuO_5 (1–4) and Nd_2BaZnO_5 (11–13) is tetragonal. However, these two compounds belong to two different space groups, namely, $P4/mbm$ (D_{4h}^5) and $I4/mcm$ (D_{4h}^{18}), respectively. In both compounds, the Nd^{3+} ion is located at the center of a trigonal prism formed by the O(2) atoms whereas two of the three rectangular faces are capped by O(1) atoms. The point group is C_{2v}. Figure 1a schematically shows the NdO_8 polyhedron. Neodymium–oxygen distances are very close for both compounds (see Table 1). The coordination polyhedra of four neodymium atoms compose a Nd_4O_{21} unit around one O(1) atom common for all the four NdO_8 polyhedra (see Fig. 1b). There are Nd–O layers perpendicular to the c axis. Ba^{2+} and Cu^{2+} (or Zn^{2+}) ions are situated between two successive Nd–O layers and are surrounded by ten and four oxygen atoms, respectively. While there is only one Nd–O layer in the unit cell of Nd_2BaCuO_5, there are two such layers in the unit cell of Ne_2BaZnO_5, rotated by 90° around the screw axis at the Zn position. Correspondingly, the c lattice constant doubles for Nd_2BaZnO_5 as compared to that for Nd_2BaCuO_5 (see Table 1). The coordination polyhedron for Ba^{2+} is a rectangular bicapped prism in the copper compound and an antiprism in the zinc compound. The Cu^{2+} ions reside in plane rectangles (Nd_2BaCuO_5) while the Zn^{2+} ions are inside tetrahedra (Nd_2BaZnO_5).

3. EXPERIMENTAL

The X-ray single-phase polycrystalline samples were prepared from high-purity oxydes (Nd_2O_3, La_2O_3, CuO, or ZnO) and carbonate $BaCO_3$ by solid state reaction in air in a manner described earlier in Refs. (14, 18).

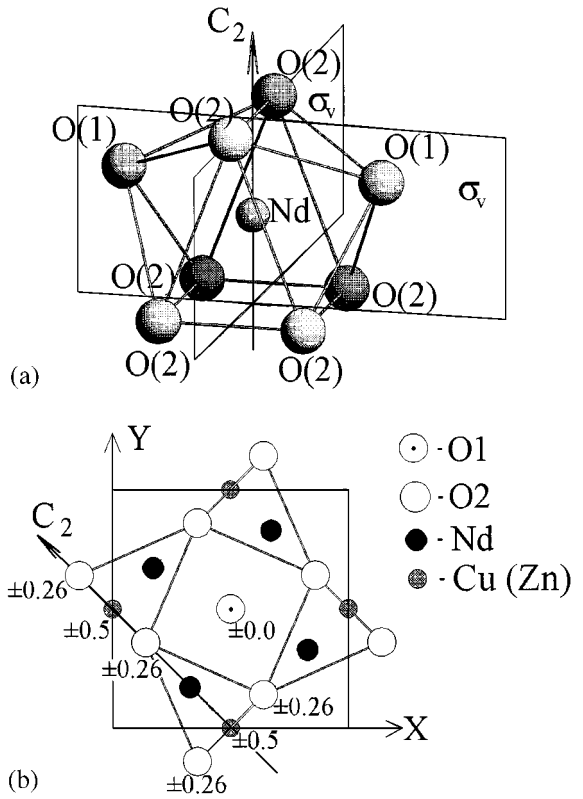

FIG. 1. Structural fragments for $Nd_2Ba\mathit{M}O_5$ (M = Cu, Zn) reconstructed using the atomic positions from Refs. (3, 14). (a) The NdO_8 polyhedron. The C_2 axis and two mirror planes σ_v of the C_{2v} local point symmetry group are indicated. (b) XY projection of the Nd_4O_{21} unit in the crystal structure.

Diffuse transmittance spectra of Nd_2BaCuO_5 power samples at the temperatures between 5 and 150 K were registered by a BOMEM DA3.002 Fourier-transform spectrometer in the spectral region 1800–18,000 cm^{-1} with the resolution 2 cm^{-1}.

Absorption of Nd_2BaZnO_5 was measured in the spectral region between 3700 and 34,000 cm^{-1} using a Cary 3400 grating spectrometer and/or a 3.4 Jarrell-Ash grating spec-

TABLE 1
Nd–O Distances and Lattice Constants (in nm) in $Nd_2Ba\mathit{M}O_5$

	M = Cu [3]	M = Zn [14]
Nd–O(1) (×2)	0.248	0.249
Nd–O(2) (×2)	0.232	0.230
Nd–O(2) (×4)	0.259	0.263
a	0.670	0.675
c	0.582	1.154

trograph. The Nd^{3+} crystal field levels of the ground $^4I_{9/2}$ and the first excited $^4I_{11/2}$ states were determined from the emission spectra of 1% Nd^{3+}: La_2BaZnO_5 samples in the 850 to 1150 nm wavelength range. Fluorescence coming from the $^4F_{3/2}$ level has been induced by 514.5-nm argon ion laser excitation and the spectrum was dispersed using a 1-m double-spectrometer HR 1000 Jobin-Yvon equipped with a 1200 grooves/mm grating. The signal was detected by a cooled Hamamatsu 928 photomultiplier. The absorption measurements of zinc compounds were performed for the sample temperatures 4.2, 77, and 300 K.

4. EXPERIMENTAL RESULTS

Figure 2 shows the observed electronic transitions of the Nd^{3+} ions in Nd_2BaCuO_5 in the 2000- to 15,000-cm^{-1} spectral domain. For a comparison, gray boxes indicate the appropriate spectra of Nd^{3+} in the LaF_3 matrix in the same spectral regions (data from Ref. (19)). While the crystal field levels of the low-lying Nd^{3+} multiplets $^4I_{11/2}$, $^4I_{13/2}$, and $^4I_{15/2}$ are in the same energy intervals for both Nd_2BaCuO_5 and LaF_3, higher energy crystal field manifolds for Nd_2BaCuO_5 are shifted to the low-energy side in comparison with their position in LaF_3:Nd^{3+}. This nephelauxetic shift (20–22) is due to a greater overlap of the Nd^{3+} excited state wave functions with ligand wave functions in Nd_2BaCuO_5. The same is observed for Nd_2BaZnO_5.

Figure 3 displays the spectra of Fig. 2 in more detail. Positions of crystal field levels of the excited multiplets are indicated by arrows above the spectrum. Spectral lines corresponding to the transition from the first excited crystal field level of the ground multiplet are shown by arrows below the spectrum. We were able to identify the spectral lines originating from the thermally populated levels of the ground multiplet in the absorption spectra taken at different temperatures. The data on Nd_2BaZnO_5 from our absorption and luminescence measurements together with data from Refs. (16, 17) are represented in Fig. 3 by vertical bars. The inspection of the lowest energy transitions $^4I_{9/2} \rightarrow {}^4I_{11/2}$, $^4I_{13/2}$, $^4I_{15/2}$ shows that, within the precision of the measurements on Nd_2BaZnO_5, the positions of energy levels coincide for the copper and zinc compounds. We consider the extra levels situated at 5722 and 5842 cm^{-1}, reported in Refs. (16, 17) and indicated by circles in Fig. 3c, to be erroneous, probably due to impurity. The lines 4133, 14,516, and 16,889 cm^{-1} (17) (also indicated by circles in Figs. 3b, 3g, and 3h) come from the thermally populated first excited state. The experimentally measured level positions for both Na_2BaZnO_5 and Nd_2BaCuO_5 are summarized in Table 2.

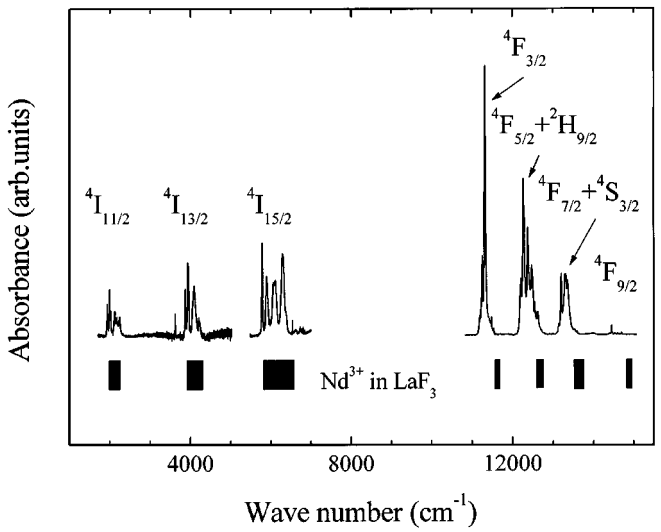

FIG. 2. Infrared absorption spectrum of Nd^{3+} in Nd_2BaCuO_5 at the temperature of 50 K. The energy intervals occupied by the crystal field levels of Nd^{3+} in LaF_3 (gray boxes) were taken from Ref. (19).

Antiferromagnetic ordering of Nd_2BaCuO_5 at $T_N = 7.5$ K (18, 4) results in splitting of the Nd^{3+} Kramers doublets and, hence, of the spectral lines (see Fig. 4). Due to quasi-one-dimensional magnetic correlation well persistent above T_N (18), these splittings are seen in Figs. 3 and 4 for some spectral lines at 9, 11, 14, and even 15 K. The split spectral lines of Nd_2BaCuO_5 narrow dramatically at T_N, while neither splittings nor a narrowing of spectral lines is observed in Nd_2BaZnO_5 (see Figs. 4 and 5). The temperature dependencies of the splitting and the half-width of the spectral line at 5780 cm^{-1}, shown in Fig. 5, confirm the establishment of a magnetic order in Nd_2BaCuO_5 below T_N. The half-width of the same line for Nd_2BaZnO_5 also shown in Fig. 5 does not experience any changes, which proves that no magnetic ordering occurs in this compound down to the lowest measured temperature of 4.2 K. The splittings of Nd^{3+} ion Kramers doublets in an ordered state of Nd_2BaCuO_5 deduced from the low-temperature spectra are listed in Table 2.

5. CRYSTAL FIELD CALCULATIONS AND DISCUSSION

As has already been mentioned in the previous section, the positions of Nd^{3+} crystal field levels in the energy region between 2000 and 17,500 cm^{-1} coincide for Nd_2BaCuO_5 and Nd_2BaZnO_5. This fact gives us a reason to perform only one fitting procedure for both compounds and to use in it the experimental data on the zinc compound for energies higher than 17,500 cm^{-1} (see Table 2). The simulation is performed on the basis of the crystal field theory considering 182×182 Kramer's doublet of $4f^3$ configuration. In the central ion approximation the rare earth ion, R^{3+}, is submitted to different interactions. First of all, the free ion Hamiltonian can be reproduced by 20 phenomenological parameters, e.g., 4 Racah's (E^0, E^1, E^2, E^3), spin–orbit coupling constant (ζ), Trees' (α, β, and γ), and 6 Judd's (T^{λ}

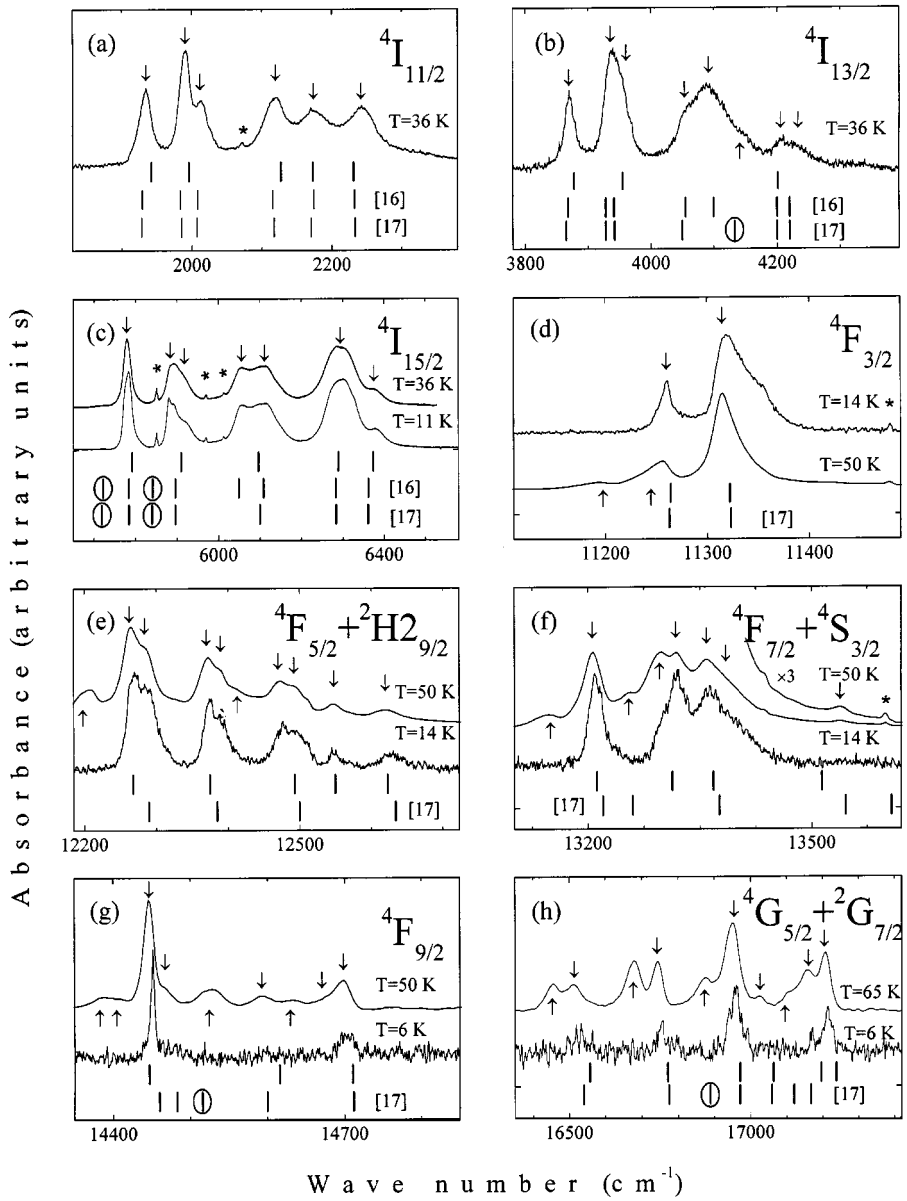

FIG. 3. Electronic transitions from the ground $^4I_{9/2}$ level of Nd^{3+} in Nd_2BaCuO_5 to the low-lying excited levels. Spectral lines due to some additional phase are marked by asterisks. For further explanations, see the text.

parameters). Extra magnetic interactions are also considered through the M^k and P^i-parameters, even if their values are fixed to standard values and/or ratios. The Hamiltonian is written as follows:

$$H_{FI} = H_0 + \sum_{k=0,1,2,3} E_k e^k + \zeta_{4f} A_{SO} + \alpha L(L+1) + \beta G(G_2) + \gamma G(R_7) + \sum_{\lambda=2,3,4,6,7,8} T^\lambda t_\lambda + \sum_{k=0,2,4} M^k m_k + \sum_{i=2,4,6} P^i p_i.$$

Furthermore, the electric field produced by the surrounding ligands, described in the frame of Wybourne's formalism (23), depends on the site point symmetry around the R^{3+} ion. The local symmetry for the neodymium ions in both title compounds is C_{2v}, which implies nine crystal field parameters.

$$H_{CF}(C_{2v}) = B_0^2 + B_0^4 + B_0^6 + B_2^2(C_2^2 + C_{-2}^2) + B_2^4(C_2^4 + C_{-2}^4) + B_2^6(C_2^6 + C_{-2}^6) + B_4^4(C_4^4 + C_{-4}^4) + B_4^6(C_4^6 + C_{-4}^6) + B_6^6(C_6^6 + C_{-6}^6).$$

TABLE 2

Experimental Energy Levels, E_{exp}, Nd^{3+} in Nd_2BaMO_5 (M = Zn, Cu) Experimental Level Splittings in a Magnetically Ordered Nd_2BaCuO_5, ΔE_{exp}, and Calculated Energy Levels (with Parameters from Table 3) and Corresponding Magnetic g-Factors

	Experiment			Calculations			
	Nd_2BaZnO_5	Nd_2BaCuO_5					
Level[a]	E_{exp} (cm^{-1})	E_{exp} (cm^{-1})	ΔE_{exp} (cm^{-1})	E_{calc} (cm^{-1})	g_x	g_y	g_z
1	2	3	4	5	6	7	8
$^4I_{9/2}$	0	0	7	0.8	− 2.21	− 0.86	4.46
	67	64		79	− 1.01	− 4.40	1.59
	228	—		231	− 1.28	1.01	− 1.29
	287	—		306	2.81	3.04	1.09
	460	—		476	− 1.95	− 2.47	− 2.53
$^4I_{11/2}$	1942	1935	8	1917	− 1.94	− 0;.25	− 8.47
	1996	1991	≤ 1	1987	0.92	9.23	− 0.06
	—	2012	18	2005	5.71	2.32	0.53
	2127	2120		2126	− 3.58	− 4.59	1.22
	2173	2174		2179	− 3.29	− 6.92	0.26
	2231	2242	7	2241	4.14	6.00	1.30
$^4I_{13/2}$	3878	3870	4	3849	− 1.87	− 0.68	12.40
	—	3936	6	3926	− 1.32	− 12.14	− 0.49
	3955	3961	≤ 2	3943	− 8.61	0.38	− 0.20
	—	4054		4060	8.44	− 1.47	1.34
	—	4092		4094	− 0.82	9.41	− 1.91
	4202	4206		4204	− 1.62	6.93	− 4.83
	—	4234		4233	− 1.87	− 10.13	1.05
$^4I_{15/2}$	5792	5779	7	5777	1.56	0.03	− 15.54
	5911	5890		5905	0.09	16.22	− 0.63
	—	5914		5933	12.89	1.85	1.61
	—	6057		6037	− 6.20	− 8.75	1.14
	6097	6112		6117	− 5.42	− 8.50	− 3.44
	6289	6295		6298	9.22	4.28	2.94
	—	—		6348	− 3.14	12.94	− 1.93
	6373	6376		6363	0.53	− 8.51	6.43
$^4F_{3/2}$	11,264	11,260	3	11,258	0.78	0.62	0.62
	11,322	11,319	32	11,312	− 0.44	− 0.44	− 1.22
$^4F_{5/2}$	12,268	12,265	8	12,254			
	—	12,281	≈ 0	12,273			
$^2H2_{9/2}$	12,375	12,373	≈ 0	12,391			
	—	12,472	1.5	12,454			
	—	12,491		12,486			
	12,493	12,548		12,551			
	12,550	—		12,572			
	12,623	12620		12,627			
$^4F_{7/2}$	13,212	13,206	6	13,212			
	13,313	13,318	≈ 0	13,307			
	13,368	13,359	7	13,358			
	—	13,385		13,379			
$^4S_{3/2}$	13,514	13,539		13,540			
	—	—		13,542			
$^4F_{9/2}$	14,447	14,447	≈ 0	14,452			
	—	14,468		14,470			
	14,616	14,593		14,586			
	—	14,671		14,689			
	14,711	14,699		14,711			
$^2H2_{11/2}$	15,704[b]	—		15,794			
	15,789[b]	—		15,807			
	—	—		15,817			
	—	—		15,831			
	15,864[b]	—		15,837			

TABLE 2—*Continued*

	Experiment			Calculations			
	Nd_2BaZnO_5	Nd_2BaCuO_5					
Level[a]	E_{exp} (cm^{-1})	E_{exp} (cm^{-1})	ΔE_{exp} (cm^{-1})	E_{calc} (cm^{-1})	g_x	g_y	g_z
1	2	3	4	5	6	7	8
	15,887[b]	—		15,867			
$^4G_{5/2}$	16,540	16,514		16,553			
	16,776	16,743		16,771			
	16,971	16,955		16,965			
$^2G_{7/2}$	—	17,026		17,015			
	17,063	—		17,084			
	17,195	17,161		17,176			
	17,237	17,205		17,211			
$^4G_{7/2}$	18,556	—		18,569			
	18,591	—		18,602			
	18,639	—		18,665			
	18,897	—		18,898			
$^2K_{13/2}$	19,062	—		19,046			
	19,098	—		19,097			
$^4G_{9/2}$	—	—		19,137			
	—	—		19,145			
	19,170	—		19,198			
	19,248	—		19,234			
	19,275	—		19,263			
$^2K_{13/2}$	—	—		19,360			
	19,496	—		19,492			
	—	—		19,550			
	19,612	—		19,631			
	—	—		19,643			
$^2K_{15/2}$	20,555	—		20,551			
$^2G1_{9/2}$	20,592	—		20,569			
	20,660	—		20,659			
	20,703	—		20,717			
$^2D1_{3/2}$	20,845	—		20,849			
	—	—		20,897			
$^4G_{11/2}$	20,927	—		20,917			
$^2G1_{9/2}$	—	—		20,953			
$^4G_{11/2}$	20,969	—		20,962			
$^2K_{15/2}$	—	—		21,101			
	—	—		21,136			
$^4G_{11/2}$	21,193	—		21,208			
$^2K_{15/2}$	21,255	—		21,296			
$^4G_{11/2}$	21,321	—		21,334			
$^2K_{15/2}$	—	—		21,425			
$^4G_{11/2}$	—	—		21,450			
	21,483	—		21,474			
$^2K_{15/2}$	—	—		21,523			
	—	—		21,567			
	—	—		21,620			
	21,649	—		21,636			
$^2P_{1/2}$	22,930	—		22,937			
$^2D1_{5/2}$	23,443	—		23,467			
	23,482	—		23,486			
	23,620	—		23,599			
$^2P_{3/2}$	25,797	—		25,808			
	25,880	—		25,856			
$^4D_{3/2}$	27,245	—		27,239			
	27,487	—		27,467			
$^4D_{5/2}$	27,616	—		27,652			

TABLE 2—*Continued*

	Experiment			Calculations			
	Nd_2BaZnO_5	Nd_2BaCuO_5					
Level[a]	E_{exp} (cm^{-1})	E_{exp} (cm^{-1})	ΔE_{exp} (cm^{-1})	E_{calc} (cm^{-1})	g_x	g_y	g_z
1	2	3	4	5	6	7	8
$^4D_{3/2}$	27,714	—		27,703			
$^4D_{5/2}$	—	—		27,807			
$^4D_{1/2}$	28,069	—		28,054			
$^2I_{11/2}$	28,503	—		28,508			
	28,514	—		28,513			
	—	—		28,724			
	—	—		28,843			
	—	—		29,058			
	29,135	—		29,124			
$^2L_{15/2}$	—	—		29,382			
	—	—		29,443			
	—	—		29,608			
	—	—		29,615			
$^4D_{7/2}$	—	—		29,670			
$^2L_{15/2}$	—	—		29,698			
$^4D_{7/2}$	29,711	—		29,717			
$^2L_{15/2}$	—	—		29,777			
$^4D_{7/2}$	—	—		29,913			
$^2I_{13/2}$	—	—		29,925			
$^4D_{7/2}$	—	—		29,953			
$^2L_{15/2}$	29,953	—		29,961			
$^2I_{13/2}$	—	—		29,974			
	30,018	—		30,025			
$^2I_{13/2}$	—	—		30,083			
	—	—		30,179			
	—	—		30,216			
	—	—		30,412			
	—	—		30,444			
$^2L_{17/2}$	—	—		30,860			
	—	—		30,930			
	—	—		31,099			
	—	—		31,153			
	—	—		31,174			
	—	—		31,240			
	—	—		31,282			
	—	—		31,428			
	—	—		31,449			
$^2H1_{9/2}$	—	—		32,164			
	—	—		32,194			
	—	—		32,292			
	—	—		32,317			
	—	—		32,366			
$^2D2_{3/2}$	32,587	—		32,608			
	32,780	—		32,761			
$^2H1_{11/2}$	—	—		33,484			
$^2D2_{5/2}$	—	—		33,563			
$^2H1_{11/2}$	33,616	—		33,617			
	—	—		33,649			
	—	—		33,707			
$^2D2_{5/2}$	—	—		33,736			
	—	—		33,762			
$^2H1_{11/2}$	—	—		33,808			
	—	—		33,856			

[a]The level that gives the biggest contribution to the wave function.
[b]Not used for calculations.

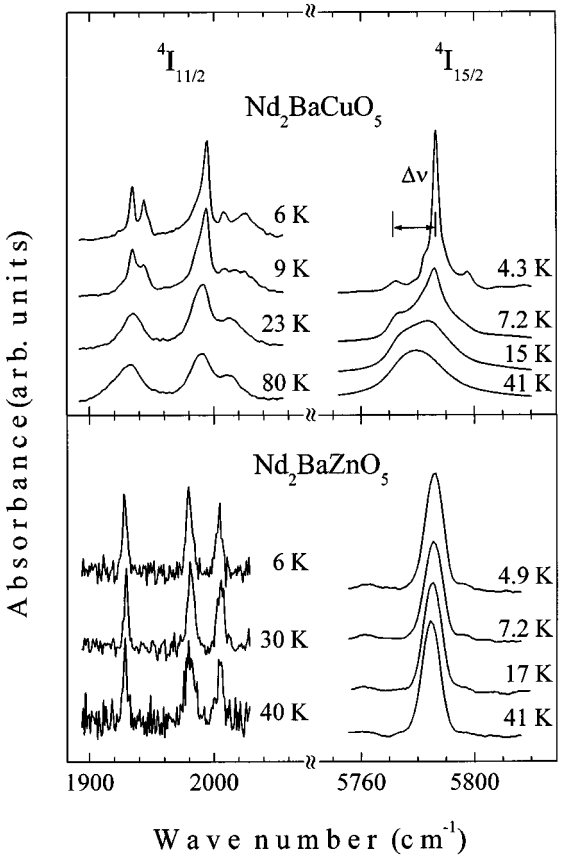

FIG. 4. The lowest frequency part of $^4I_{9/2} \rightarrow {}^4I_{11/2}$ and $^4I_{9/2} \rightarrow {}^4I_{15/2}$ transitions in Nd_2BaCuO_5 and Nd_2BaZnO_5 at different temperatures.

A starting set of the free-ion and crystal field parameters is from Ref. (15). The best parameter set is listed in Table 3. The final mean deviation, taken as a figure of merit, is 13.7 cm^{-1}. This result is good. However, we have some problems with the $^2H2_{9/2}$ level and this level is not used in the initial fitting procedure. In fact, there is some ambiguity between the experimental data and the simulation. The $^2H2_{9/2}$ level is situated near the $^4F_{5/2}$ level and the highest $^4F_{5/2}$ sublevel is found at 12,373 cm^{-1}. In the high-resolution absorption spectrum recorded at low temperature, there is a shoulder at about 12,386 cm^{-1} on the upper energy side of that line. It may correspond to the lowest Stark component of the next excited level $^2H2_{9/2}$, giving the following order of five $2J + 1$ sublevels in increasing energy position: 1-2-1-1 ("2" means two sublevels very close to one another). But in the final simulation this order is 2-2-1. Moreover, the lowest Stark level of the $^2H2_{9/2}$ level is calculated at 12,454 cm^{-1}, almost 70 cm^{-1} higher than the supposed experimental one. Nevertheless, we may consider that this shoulder at 12,386 cm^{-1} in fact is not the lowest $2H2_{9/2}$ sublevel. Then, instead of it, we can take a line situated at 12,472 cm^{-1} as the first Stark component of the $^2H2_{9/2}$ level, and the order of sublevels should be 2-1-?-1, with one missing component in the absorption spectrum. In

TABLE 3
Free Atom and Crystal Field Parameters for Nd^{3+} (For More Details See Text); Values in cm^{-1}

Parameter	$Nd_2Ba(Zn/Cu)O_5$
E^0	23312.54
E^1	4885.99
E^2	22.71
E^3	474.03
α	20.47
β	− 701.85
γ	[750.00]
T^2	276.94
T^3	78.26
T^4	61.18
T^6	− 277.94
T^7	262.18
T^8	239.78
ζ	868.77
M^0	1.73
M^2	0.97
M^4	0.65
P^2	286.10
P^4	214.57
P^6	143.06
B_0^2	481
B_2^2	44
B_0^4	843
B_2^4	534
B_4^4	1734
B_0^6	966
B_2^6	180
B_4^6	201
B_6^6	− 7
Number of exp. levels	93
Residue	17,451.3 cm^{-2}
r.m.s. deviation	13.7

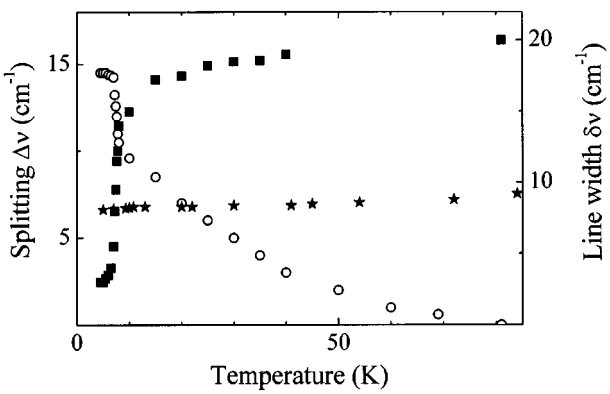

FIG. 5. Temperature dependencies of the splitting (circles) of the lowest frequency line in the $^4I_{9/2} \rightarrow {}^4I_{15/2}$ transition in the Nd^{3+} ion in Nd_2BaCuO_5 and the half-widths of the same line for Nd_2BaCuO_5 (squares) and Nd_2BaZnO_5 (stars).

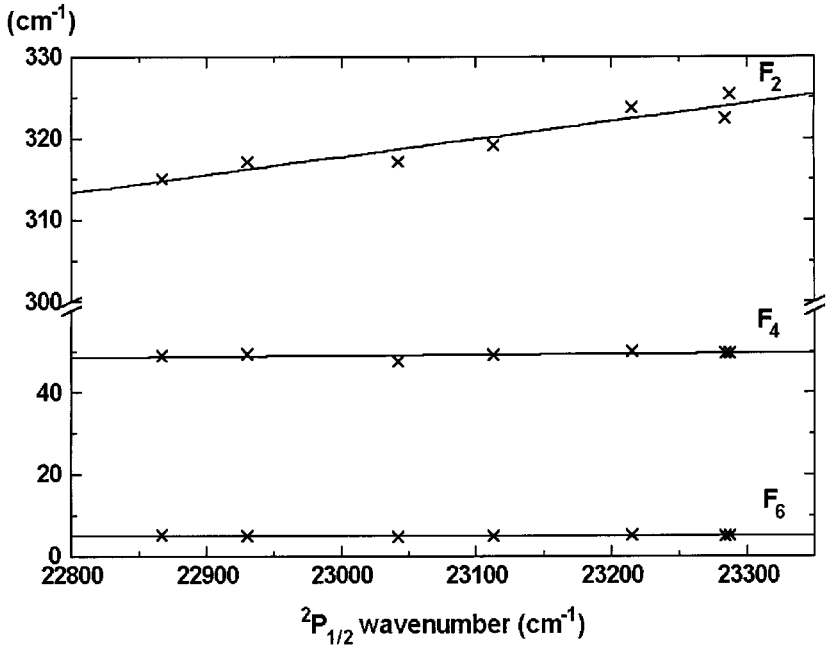

FIG. 6. Slater–Condon integrals as a function of $^2P_{1/2}$ level position in various neodymium compounds (see Table 4).

that case, the overall splitting of the $^2H2_{9/2}$ level is comparable to the calculated one obtained using the phenomenological crystal field parameters from Table 3. It should be mentioned that the distance between the shoulder at 12,386 cm^{-1} and the lowest Stark level of the $^4F_{5/2}$ multiplet is close to the energy 117 cm^{-1} of the lowest frequency optical phonon in Nd_2BaCuO_5 (24). So the shoulder at 12,386 cm^{-1} could be a phonon replica of the zero-phonon line at 12,265 cm^{-1}.

The positions of the electronic levels depend on the free-ion parameter's magnitude moving theirs barycenter's positions along the energy scale. The Racah's parameters E^k's are the linear combination of Slater's integrals F_k's (23). Figure 6 shows the F_k values as a function of the $^2P_{1/2}$ energy level position for different crystalline compounds (Table 4). This is a test for Racah's parameters given in Table 3. And, as is clear from the curves displayed in Fig. 6, the linear evolution of the Slater–Condon integrals confirms that the parameters derived in this study are in agreement with the F_k values previously given in the literature. The "barycenter curves" have already been used for testing the energy level positions of different rare earth ions along the lanthanide series (25).

Wave functions obtained from the described crystal field calculations were used to calculate the magnetic g-factors. They are listed in columns 6 and 7 of Table 2. As the copper compound orders magnetically but the zinc one does not, it is evident that the exchange splittings of the Nd^{3+} levels result, mainly, from the neodymium–copper interactions. The most simple way to account for these interactions would be to introduce an effective magnetic field $\vec{H}_{eff}$ created by the ordered Cu^{2+} magnetic moments and to find splittings from the above-calculated g-factors. It is easy to see that it is not possible to introduce such an effective field

TABLE 4
Slater–Codon Integrals and $^2P_{1/2}$ Energy Position in Some Crystalline Compounds: Values in cm^{-1}

F_k	A–Nd_2O_3 (26)	Nd_2BaMO_5 (M = Zn, Cu) This work	YVO_4:Nd^{3+} (27)	$LuAlO_3$:Nd^{3+} (28)	$LaCl_3$:Nd^{3+} (29)	$NdAlO_3$ (29)	Nd[diph][a] (30)
F_2	315.1	317.19	317.18	319.2	323.8	322.5	325.47
F_4	49.13	49.48	47.74	49.22	50.17	49.77	49.72
F_6	5.22	5.117	4.78	5.09	5.21	5.13	5.169
$^2P_{1/2}$	22,867	22,930	23,042	23,113	23,215	23,284	23,287

[a]Nd[diph] = $NdH[O_3P(CH_2)_3PO_3]$.

that would reasonably describe the observed exchange splittings of Nd^{3+} Kramers doublets in a magnetically ordered copper compound (column 4 of Table 2). This fact points to a considerable contribution of anisotopic interactions. Symmetry related two-electron operators should be used to account for an anisotropic nature of the exchange splittings (31).

6. CONCLUSION

The absorption spectra of Nd^{3+} ions in two stoichiometric compounds, Nd_2BaCuO_5 and Nd_2BaZnO_5, have been analyzed. The positions of electronic transitions of neodymium ions in both compounds coincide, giving us the argument to perform only one fitting procedure on the common energy level scheme. The mean deviation of $13.7\,cm^{-1}$ is achieved in the final set. Some discrepancy between the experimental data reported previously on the ^4I multiplet in Nd_2BaZnO_5 (16, 17) and our data exists and is discussed. A comparison between the measured exchange splittings of Nd^{3+} Kramers doublets in a magnetically ordered Nd_2BaZnO_5 and the calculated magnetic g-factors reveal anisotropic character of the exchange interactions.

ACKNOWLEDGMENTS

The synthesis of Nd_2BaZnO_5 by B. V. Mill and of $(La_{1-x}Nd_x)_2BaZnO_5$ by M. Taibi is greatly acknowledged. This work was supported in part by Grant 2631 in the framework of the CNRS-RAS cooperation program and by Grant 98-02-17620a of the Russian Fund for Basic Research.

REFERENCES

1. C. Michel, L. Er-Rakho, and B. Raveau, *J. Solid State Chem.* **39,** 161 (1981).
2. C. Michel, L. Er-Rakho, and B. Raveau, *Rev. Chim. Minér.* **21,** 85 (1984).
3. J. K. Stalick and W. Wong-Ng, *Mater. Lett.* **9,** 401 (1990).
4. I. V. Golosovsky, P. Böni, and P. Fischer, *Phys. Lett. A* **182,** 161 (1993).
5. C. Michel and B. Raveau, *J. Solid State Chem.* **43,** 73 (1982).
6. N. I. Agladze, G. G. Chepurko, M. N. Popova, and E. P. Hlybov, *Pis'ma Zh. Eksp. Teor. Fiz.* **48,** 43 (1988) [*JETP Lett.* **48,** 45 (1988)]; *Phys. Lett. A* **133,** 260 (1988).
7. M. N. Popova and G. G. Chepurco, *Pis'ma Zh. Eksp. Teor. Fiz.* **52,** 1157 (1990). [*JETP Lett.* **52,** 562 (1990)]
8. I. V. Paukov, M. N. Popova, and B. V. Mill, *Phys. Lett. A* **169,** 301 (1992).
9. M. N. Popova, S. A. Klimin, E. Antic-Fidancev, P. Porcher, M. Taibi, and J. Aride, *J. Alloys Compd.* **284,** 138 (1999).
10. C. Michel and B. Raveau, *J. Solid State Chem.* **49,** 150 (1983).
11. M. Taïbi. "Contribution à l'étude cristallochimique, magnétique et optique des phases $Ln_2MM'O_5$." Thesis, Rabat, Morocco, 1990.
12. C. Michel, L. Er-Rakho, and B. Raveau, *J. Solid State Chem.* **42,** 176 (1982).
13. M. Taïbi, J. Aride, J. Darriet, A. Moqine, and A. Boukhari, *J. Solid State Chem.* **86,** 233 (1990).
14. M. Taïbi, J. Aride, E. Antic-Fidancev, M. Lemaître-Blaise, P. Porcher, and P. Caro, *J. Solid State Chem.* **74,** 329 (1988).
15. M. Taïbi, J. Aride, E. Antic-Fidancev, M. Lemaître-Blaise, and P. Porcher, *Phys. Stat. Sol.* (*a*) **115,** 523 (1989).
16. A. de Andrés, S. Taboada, J. L. Martínez, M. Dietrich, A. Litvinchuk, and C. Thomsen, *Phys. Rev. B* **55,** 3568 (1997).
17. B. Dareys, P. Thurian, M. Dietrich, M. V. Abrashev, A. P. Litvinchuk, C. Thomsen, A. De Andrés, and S. Taboada, *Phys. Rev. B* **55,** 6871 (1997).
18. I. V. Paukov, M. N. Popova, and B. V. Mill, *Phys. Lett. A* **157,** 306 (1991).
19. A. A. Kaminskii, "Crystalline lasers: physical processes and operating schemes." CRC Press, Boca Raton, FL, 1996.
20. P. Caro, O. Beaury, and E. Antic, *J. Phys.* **37,** 671 (1976).
21. P. Caro, E. Antic, L. Beaury, O. Beaury, J. Derouet, M. Faucher, C. Guttel, O. K. Moune, and P. Porcher, "Colloques Internationaux du Centre National de la Recherche Scientifique: Spectroscopie des Éléments de Transition et des Éléments Lourds dans les Solids," CNRS France **255,** p. 71. Paris, 1977.
22. E. Antic-Fidancev, M. Lemaître-Blaise, and P. Caro, *New J. Chem.* **11,** 467 (1987).
23. B. G. Wybourne, "Spectroscopic Properties of Rare Earths." Wiley, New York, 1965.
24. S. Taboada, A. de Andrés, J. L. Martínez, R. P. S. M. Lobo, P. Odier, F. Gervais, A. Salinas, and R. Saez-Puche, *J. Alloys. Compd.* **225,** 218 (1995).
25. E. Antic-Fidancev, *J. Alloys Compd.* **300–301,** 2 (2000).
26. P. Caro, J. Derouet, L. Beaury, and E. Soulie, *J. Chem. Phys.* **70,** 2542 (1979).
27. O. Guillot-Noel, A. Kahn-Harari, B. Viana, D. Vivien, E. Antic-Fidancev, and P. Porcher, *J. Phys.: Condens. Matter* **10,** 6491 (1998).
28. M. Faucher, D. Garcia, E. Antic-Fidancev, and M. Lemaître-Blaise, *J. Phys. Chem. Solids* **50,** 1227 (1989).
29. P. Caro, D. R. Svoronos, E. Antic, and M. Quarton, *J. Chem. Phys.* **66,** 5284 (1977).
30. E. Antic-Fidancev, F. Serpaggi, and G. Férey, *J. Alloys Compd.* **319,** 140 (2001).
31. R. L. Cone and R. S. Meltzer, *in* "Spectroscopy of solids containing rare earth ions" (A. A. Kaplyanskii and R. M. Macfarlane, Eds.), Chap. 8, p. 481. North-Holland, Amsterdam, 1987.